High-temperature corrosion of aluminized-AISI 1020 steel with NaCl and Na2SO4 deposits

By Muhammad Badaruddin

WORD COUNT 4729
TIME SUBMITTED 26-FEB-2020 08:22AM
PAPER ID 55895299

Bull. Mater. Sci. (2020) 43:11
https://doi.org/10.1007/s12034-019-1984-0

High-temperature corrosion of aluminized-AISI 1020 steel with NaCl and Na_2SO_4 deposits

M BADARUDDIN[1,*], SUGIYANTO[1] and D ASMI[2]

[1]Department of Mechanical Engineering, Faculty of Engineering, Universitas Lampung, Bandar Lampung 35145, Indonesia

[2]Department of Physics, Faculty of Mathematics and Natural Science, Universitas Lampung, Bandar Lampung 35145, Indonesia

*Author for correspondence (mbruddin@eng.unila.ac.id)

MS received 27 August 2018; accepted 10 July 2019

Abstract. High-temperature corrosion of aluminized-American Iron and Steel Institute (AISI) 1020 steel with sodium chloride (NaCl) and sodium sulphate (Na_2SO_4) deposits was studied using isothermal oxidization in a dry air environment at 700°C for 49 h. NaCl and Na_2SO_4 deposits on the aluminide layer interfered with protective alumina/aluminium oxide (Al_2O_3) scale formation on the steel substrate. Chlorine and sulphur gases (Cl_{2g} and S_g, respectively) released into the atmosphere corroded the protective Al_2O_3 layer. Corrosion of the Al_2O_3 layer was also due to local formation of iron oxide (Fe_2O_3). Fe_2O_3 growth is attributed to ferric chloride ($FeCl_3$) vaporization. S_g diffusion into the Al_2O_3 scale *via* Al^{3+} vacancy defects led to the formation of aluminium sulphide on the aluminide layer surface. Cl and S consequently induced hot corrosion of the aluminized steel, thereby increasing cyclic oxychloridation and sulphidation rates at high temperatures.

Keywords. Aluminized 1020 steel; hot corrosion; oxychloridation; sulphidation; alumina/aluminium oxide (Al_2O_3).

1. Introduction

Cold-rolled American Iron and Steel Institute (AISI) 1020 steel is a material suitable for engineering components because of its relatively low cost compared with that of high-alloy steel. This steel is used in heat exchangers, oil gas tanks, high-pressure water pipes and other equipment for fossil fuel power plants. Alkali metal sulphates produced by low-grade fuel combustion react with sodium chloride (NaCl) from ocean breezes at elevated temperatures, forming sodium sulphate (Na_2SO_4), which severely corrodes the material by oxidation, sulphidation or chloridation, thus rendering it prone to hot corrosion [1–3]. Therefore, the presence of NaCl and Na_2SO_4 deposits on engineering material components at high temperatures causes rapid degradation of the material [4,5]. In this regard, hot-dipped aluminide steel has great potential in engineering components for harsh environments. Several studies have reported that the aluminium (Al) coating and its alloys can improve carbon steel resistance to oxidation at high temperatures [6–8]. The aluminide layer on steel can supply Al atoms and form a protective aluminium oxide (Al_2O_3) layer.

To widen the application range and service life of aluminide steel, hot-corrosion behaviour and its related mechanism must be characterized. Therefore, we studied the effects of NaCl and Na_2SO_4 deposits on the surfaces of aluminized and bare steel (AS and BS) by isothermally oxidizing them at 700°C for 49 h in a static-air environment. The corrosion kinetics was analysed to determine the parabolic rate constant of corrosion (k_p). Oxidized AS samples were characterized by both optical and scanning electron microscopy (OM and SEM, respectively), energy dispersive X-ray spectroscopy (EDS) and X-ray diffraction (XRD) to determine the possible corrosion causing mechanisms.

2. Experimental

2.1 *Specimen preparation*

A commercial cold-rolled AISI 1020 steel plate with a chemical composition of 0.2C–0.05P–0.05S–0.5Mn (wt%; iron [Fe]-balanced) was cut into specimens with dimensions of 20 × 10 × 2 mm^3. Before Al deposition, all specimens were ultrasonically cleaned with a solution of 5% sodium hydroxide (NaOH) and 10% phosphoric acid (H_3PO_4) and then covered with Al welding flux pasta. Commercial Al–0.5 wt% silicon (Si) was melted in an alumina (Al_2O_3) crucible at 700°C, and the specimens were then dipped for 16 s in a molten Al bath. After the aluminizing process, oxide flux deposited on the surface of the aluminized specimens was

Published online: 17 December 2019

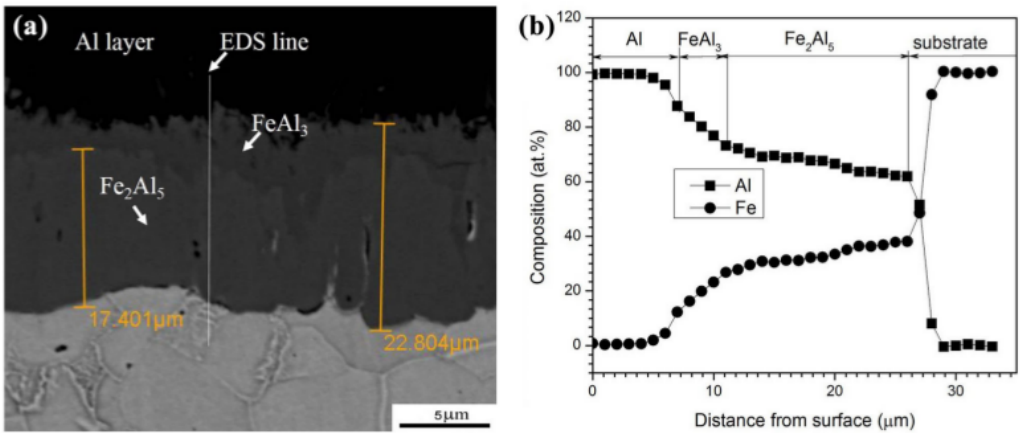

Figure 1. SEM and EDS results: (**a**) cross-sectional micrograph and (**b**) iron (Fe) and aluminium (Al) element line-scan results for aluminized AISI 1020 steel.

cleaned with a solution of nitric acid, H_3PO_4 and water (1:1:1, v/v) at room temperature.

2.2 *Corrosion testing and characterization of samples*

A saturated NaCl and Na_2SO_4 solution was sprayed onto the largest surface of each specimen placed on a 200°C hot plate to form deposits at a concentration of 2 mg cm^{-2}. A salt of NaCl and Na_2SO_4 at a concentration of 2 mg cm^{-2} was similar to that reported in the literature [9,10]. All BS and AS specimens with NaCl and Na_2SO_4 coatings were isothermally oxidized at 700°C for 1–49 h. In the present investigation, a temperature of around 700°C is referred to as type-II hot corrosion, which occurs at temperatures below that of salt melting [11].

After a given isothermal oxidation time, the specimens were removed and cooled in air at room temperature. Each data point for corrosion kinetic-related weight gain was obtained from a different specimen. Linear and parabolic plots of the weight gain (mg cm^{-2}) *vs.* oxidation time (h) were constructed. The aluminide layer thickness and microstructures of aluminized specimens were observed by OM. The phases formed on steel were identified by XRD using monochromatic Cu Kα radiation at 40 kV and 100 mA. The surface and cross-sectional morphologies of AS were examined by SEM and EDS, respectively.

3. Results and discussion

3.1 *Examination of the coated specimen*

An SEM cross-sectional micrograph and EDS element line scan for the aluminide coating and the steel substrate after the aluminizing process are displayed in figure 1a and b, respectively. When low-carbon steel and molten Al came into contact with each other during the hot-dipping process, a thin intermetallic compound (IMC) formed between the steel and aluminide layer. However, not all of the IMCs formed during the aluminizing hot-dip coating, except for the Fe_2Al_5 and $FeAl_3$ phases, could be confirmed [12].

The formation of the IMCs in the Al-rich zone suggests that inward diffusion of Fe and outward diffusion of Al predominantly controlled the phase transformation and formed an aluminide layer on the steel substrate. The thickness of the aluminide layer consisting of the Al and $FeAl_3/Fe_2Al_5$ intermetallic layers was about 50 μm ($FeAl_3$: 5.403 μm and Fe_2Al_5: 17.401 μm). This coating layer showed no cracks and voids at the interface between the aluminide layer and steel substrate. In addition, an EDS element line scanning showed that the Fe content of the Al coating was much less than that of the intermetallic layer. This may have been caused by the lower diffusion rate of Fe atoms in molten Al compared with that of Al atoms in Fe [13]. The Al content decreased while the $FeAl_3$ and Fe_2Al_5 content increased towards the steel substrate after formation of the aluminizing coating by the hot-dip process (figure 1b).

3.2 *Corrosion kinetics*

Figure 2a shows the corrosion kinetics of AS after oxidation at 700°C for 49 h in various environments. Corresponding data for BS are also included for comparison. As seen in figure 2a, BS showed a rapid weight gain for up to 49 h. As weight gain caused by NaCl deposits was slow during the initial corrosion stage (up to 9 h; 2.5 mg cm^{-2}), the rate gradually decreased to 2.1 mg cm^{-2} after 49 h of corrosion. Similarly, AS with Na_2SO_4 deposits showed a slow weight gain at 1.4 mg cm^{-2} after 49 h of corrosion. AS showed weight gains lower than those of AS specimens with NaCl and Na_2SO_4 deposits oxidized at 700°C in dry air.

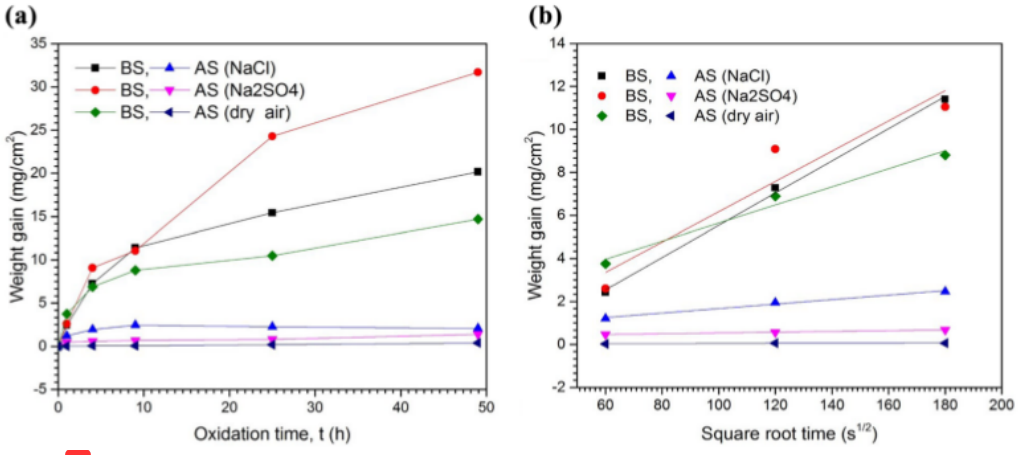

Figure 2. Corrosion kinetics of BS and aluminized AISI 1020 steel at 700°C: (**a**) linear plot at 49 h and (**b**) parabolic plot at 9 h.

Pieraggi [14] suggested that plots of a weight gain (ΔW) *vs.* $t^{1/2}$ may be a more useful and accurate analysis for the real effect on the oxidation kinetics of pure metals due to primary oxide scale growth. Therefore, plots of weight gain and square roots of time for all specimens undergoing oxidation for 9 h in the parabolic regime are displayed in figure 2b, and the parabolic rate constant (k_p) was determined by linear regression. The k_p values for BS with NaCl and Na_2SO_4 deposits were 3.721×10^{-9} and 4.122×10^{-9} g^2 cm^{-4} s^{-1}, respectively; the k_p value for BS without NaCl or Na_2SO_4 deposits oxidized in dry air was 2.735×10^{-9} g^2 cm^{-4} s^{-1}. The k_p values for AS with NaCl and Na_2SO_4 deposits were 1.082×10^{-10} and 3.204×10^{-12} g^2 cm^{-4} s^{-1}, respectively, and that for AS in dry air was 7.517×10^{-13} g^2 cm^{-4} s^{-1}. According to the k_p values, the aluminide layer on AISI 1020 steel appears to play an important role in forming a protective alumina/aluminium oxide (Al_2O_3) scale [8,15]. Consequently, k_p values for AS with NaCl and Na_2SO_4 coatings decreased by one and three orders of magnitude, respectively. These reductions are attributed to the growth of an Al_2O_3 layer, which led to the establishment of a barrier at the Al_2O_3/aluminide layer interface [16].

The oxidation rates for AS with NaCl and Na_2SO_4 deposits were three and one order(s), respectively, of magnitude higher than those of AS in dry air (figure 2b). This enhancement is attributed to the presence of gaseous chlorine (Cl_{2g}) and sulphur (S_g) from NaCl and Na_2SO_4 decomposition [1,5,7,17,18] *via* the metal-oxide reaction with Cl and S particles, which led to an active corrosion phenomenon at the Al_2O_3/aluminide coating interface. The weight gain of AS containing NaCl deposits decreased slowly at oxidation times ranging from 9 to 49 h. This low decrease may have been due to disruption of Al_2O_3 scale growth by Cl *via* cyclic oxychloridation, which forms volatile metal chlorides [7,9,19].

3.3 *Hot-corrosion mechanisms in AS*

To elucidate the hot-corrosion behaviour and phase transformation in the aluminide layer, saturated NaCl and Na_2SO_4 solutions were deposited on AS specimen surfaces, which were then isothermally oxidized at 700°C for 1–49 h. In the present study, we speculated that during the initial stages of oxidation, the kinetics was controlled by oxidation of the aluminide coating with oxygen to form Al_2O_3. In further stages of oxidation, hot corrosion occurs in which Al_2O_3 later reacts with the salt deposits and forms a mixture of salts having a lower-melting point than the original salts. The melting points of NaCl and Na_2SO_4 salts were 801 and 884°C [20], respectively. The NaCl hot-corrosion mechanisms at a 700°C appeared to be similar to those reported by Ciszak *et al* [18] and Godlewska *et al* [21]. Furthermore, the Na_2SO_4 hot-corrosion mechanisms at 700°C appear to be similar to those reported by Shi [17] and Yan *et al* [19]. Thermodynamic data for the reaction kinetics of Fe and Al in the formation of metal chlorides and sulphates were determined based on Gibbs free energy change (ΔG) calculations [22]. ΔG values at 700°C are tabulated in table 1. Table 1 shows a detailed summary of the possible chemical reactions for accelerating hot-corrosion processes of aluminide layers with NaCl and Na_2SO_4 deposits.

The cross-sectional morphologies of AS specimens with NaCl deposits hot corroded at 700°C for 1, 9 and 25 h are presented in figure 3. After 1 h of oxidation, an Fe_2Al_5/$FeAl_2$ layer and a thin FeAl layer formed on the steel substrate (figure 3a). The thickness of the aluminide layer depended on the diffusional processing at high temperatures between Al atoms from the aluminide coating and Fe atoms from the steel substrate [13], in which the diffusion coefficient of Fe into Al was 53×10^{-4} m^2 s^{-1} (520–650°C) [23], which was larger than that of Al into Fe, 1.8×10^{-4} m^2 s^{-1} (730–1400°C) [24].

Table 1. Gibbs free energy change (ΔG) of reaction [22].

	ΔG_{700} (kJ)
NaCl hot corrosion	
$2Al_{(s)} + 2NaCl_{(s)} + 2O_{2(g)} \rightarrow Al_2O_{3(s)} + Na_2O_{(s)} + Cl_{2(g)}$	−1010.4
$2Al + 3Cl_{2(g)} \rightarrow 2AlCl_{3(s)}$	−471.6
$4AlCl_{3(s)} + 3O_{2(g)} \rightarrow 2Al_2O_{3(s)} + 6Cl_{2(g)}$	−592.4
$2Fe + 3Cl_{2(g)} \rightarrow 2FeCl_{3(s)}$	−157.6
$4FeCl_{3(s)} + 3O_{2(g)} \rightarrow 2Fe_2O_3 + 6Cl_{2(g)}$	−109.3
$2Al_{(s)} + 3/2O_{2(g)} \rightarrow Al_2O_{3(s)}$	−1383.1
Na_2SO_4 hot corrosion	
$2Al_{(s)} + 3SO_{3(s)} + 3O_{2(g)} \rightarrow Al_2(SO_{4(s)})_3$	−807.0
$2Al_{(s)} + 3/2S_{(s)} \rightarrow Al_2S_3$	−676.5
$Fe_{(s)} + SO_{2(g)} + O_{2(g)} \rightarrow FeSO_{4(s)}$	−275.6
$FeSO_4 \rightarrow 1/2Fe_2O_{3(s)} + SO_{2(g)} + 1/4O_{2(g)}$	−7.2
$SO_{2(g)} + 1/2O_{2(g)} \rightarrow SO_{3(g)}$	−7.6

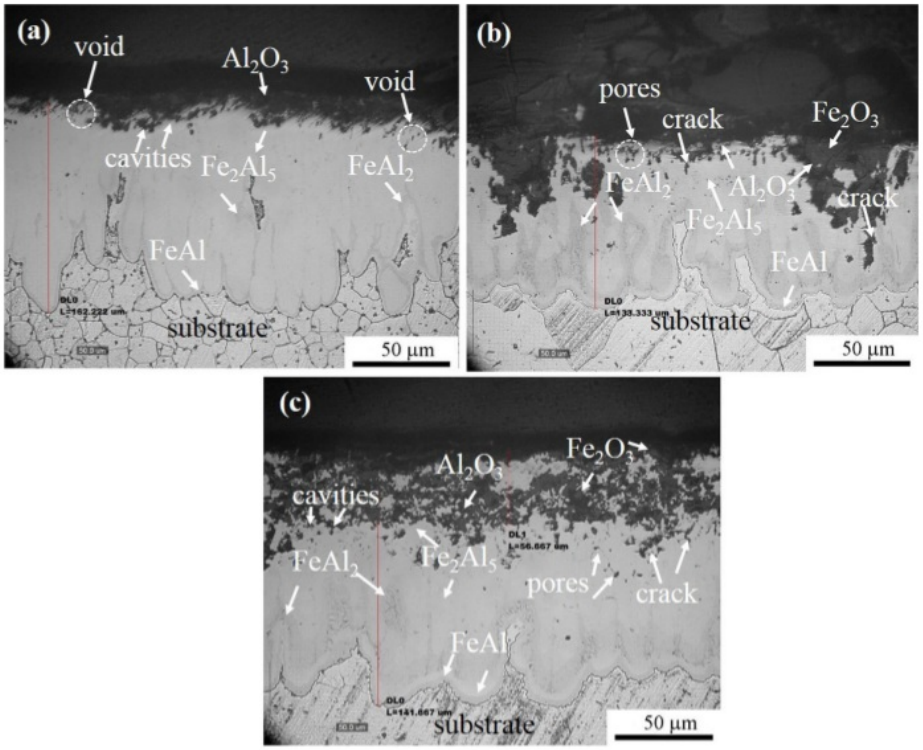

Figure 3. OM cross-sectional micrographs of AS with NaCl deposits oxidized at 700°C for (**a**) 1 h, (**b**) 9 h and (**c**) 25 h.

Therefore, the thickness of an aluminide layer was 162 µm and consisted of Fe_2Al_5, $FeAl_2$ and FeAl layers and a thin Al_2O_3 scale (figure 3a). In addition, some voids could be observed in the outer part of the aluminide layer (figure 3a) as result of outward diffusion of Al atoms to form the Al_2O_3 scale, which presented thin and dense characteristics and consisted of an adherent Al_2O_3 layer on the aluminide layer.

As the oxidation time increased to 9 and 25 h, the thickness of the $Fe_2Al_5/FeAl_2$ intermetallic layer decreased due to hot-corrosion attack in the aluminide coating (figure 3b and c). Some coarse voids and cavities formed in the outer part were filled with a mixture of oxides beneath the Al_2O_3 scale as shown in figure 3b and c. XRD examination indicated that identical intermetallic phases (Fe_2Al_5, $FeAl_2$ and

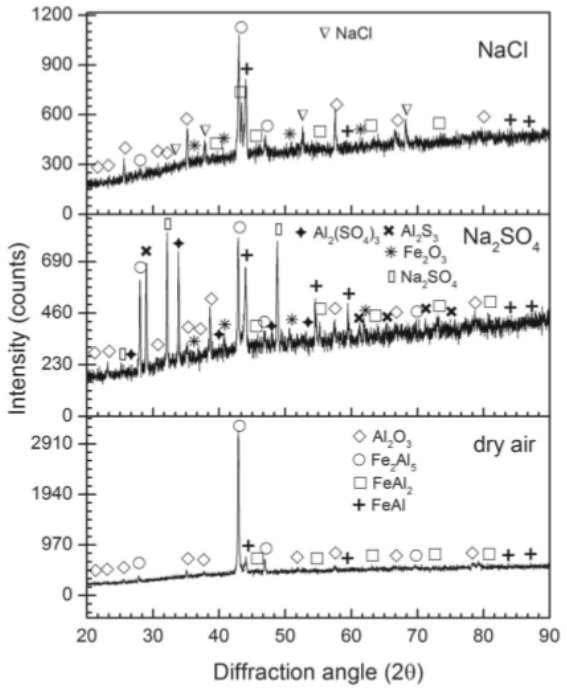

Figure 4. XRD patterns of AS specimens oxidized at 700°C for 9 h in three different environments.

FeAl) formed in the aluminide layer after oxidation of the AS specimens containing NaCl and Na_2SO_4 at 700°C during oxidation progress in an air atmosphere (figure 4). As oxidation time increased, void formation due to outward/inward Al transport predominantly formed pores in the outer part and in the aluminide layer, which is known as the Kirkendall effect [25]. Later, an interconnection of coalescing pores generated crack paths and allowed oxygen (O), Cl_{2g} and S_g penetration into the aluminide layer, forming the internal oxides (figure 3b and c). The protective Al_2O_3 layer formed during the early stages could protect the aluminide layer that was directly in contact with NaCl. However, after 25 h of corrosion, the $Fe_2Al_5/FeAl_2$ layer was severely degraded (figure 3c). This result implies that the NaCl deposit plays an important role in the hot-corrosion behaviour of the aluminide layer over long periods.

Figure 4 displays the XRD results for the AS with and without NaCl and Na_2SO_4 salt deposits, which confirmed the presence of the oxidation product, Al_2O_3 scale, together with some iron oxide (Fe_2O_3) scales. The low-intensity diffraction peaks of Al_2O_3 seen in the XRD spectrum in figure 4 were due to the thin Al_2O_3 scale on the AS specimens oxidized in air. The intensities of Al_2O_3 and Fe_2O_3 peaks for AS specimens with NaCl and Na_2SO_4 deposits increased, indicating that the corrosion layer thickened. It may be argued that Fe_2Al_5, $FeAl_2$ and FeAl can behave as Al reservoirs that maintain the growth of the Al_2O_3 scale during long-term oxidation.

As mentioned above, some pores became interconnected and resulted in crack features in which oxidant and corrosive gases consisting of O_{2g}, Cl_{2g} and sulphur trioxide (SO_{3g}) penetrated into the aluminide layer through the pores and crack paths [25]. The relative decrease in weight gains of the NaCl-deposited AS specimens during a longer oxidation time (9 h) of exposure is believed to be caused by reactions involving metal, NaCl and O, which prevented the formation of protective oxide scale. As reported by Ciszak *et al* [18], Cl_{2g} is the first major gaseous species that forms during the reaction of Na–titanium (Ti) oxides at 560°C. In the present study, the Al_2O_3 formed during the early stage could further react with NaCl and O in the gas atmosphere according to the following reaction [21]:

$$2NaCl + Al_2O_3 + 1/2O_2 \rightarrow 2NaAlO_2 + Cl_2 \quad (1)$$

Cl_{2g} was generated by the reaction among Al_2O_3, $NaCl_{(s)}$ and O_{2g} in which Na–Al oxides that readily penetrated the $Fe_2Al_5/FeAl_2$ layer through crack paths generated during oxidation were also formed. The Cl_{2g} caused corrosion of the aluminide layer, thereby forming the metal chlorides, ferric chloride ($FeCl_3$) and $AlCl_3$. Both Fe and Al were the driving forces behind metal-chloride formation in the aluminide layer during the initial stages of the reaction [7]. Furthermore, Fe and Al could have dissolved in the molten salt and volatilized or reacted with O. The melting points of $AlCl_3$ and $FeCl_3$ were 182 and 304°C, respectively [20], and their thermodynamic equilibrium Gibbs free energies at 700°C (ΔG_{700}) were about −471.6 and −157.6 kJ (table 1), respectively. The negative values of ΔG_{700} for the metal chlorides suggest that degradation of the aluminide layer was caused by the formation of Fe and Al chlorides, which are similar findings to those reported by Li *et al* [7] and Tsaur *et al* [25]. In addition, $FeCl_3$ formation was dependent on the activity of Al atoms in the aluminide layer, in which they reach lower concentrations because of their inward diffusion into the steel substrate. Metal chlorides resulted from the reaction of both Al and Fe atoms with Cl_{2g} at 700°C in the aluminide layer, thereby increasing the partial pressure of metal chlorides and forcing $AlCl_3$ and $FeCl_3$ to move towards O at high-partial pressures [7]. At the same time, Fe atoms in Fe_2Al_5 and $FeAl_2$ diffused outwards and reacted with Cl to form $FeCl_3$. Subsequently, $FeCl_3$ moved towards O at high-partial pressure, reacting again with O to form Fe_2O_3. These results are observed in the XRD scan and the SEM/EDS elemental maps (figures 4 and 5a, respectively).

SEM observation and EDS elemental mapping of the aluminide layer (figure 5a) clearly show that Cl_{2g} resulted from oxychloridation, which destroyed the protective Al_2O_3 scale on the aluminide layer [15]. Almost all of the Fe_2O_3 scales formed on the FeAl layer, and only a small portion of $FeAl_2$ remained in the aluminide layer. Fe_2O_3 and Al_2O_3 formed together above the FeAl layer as shown in figure 5a. The Al_2O_3 scale that grew was loose. During oxidation for

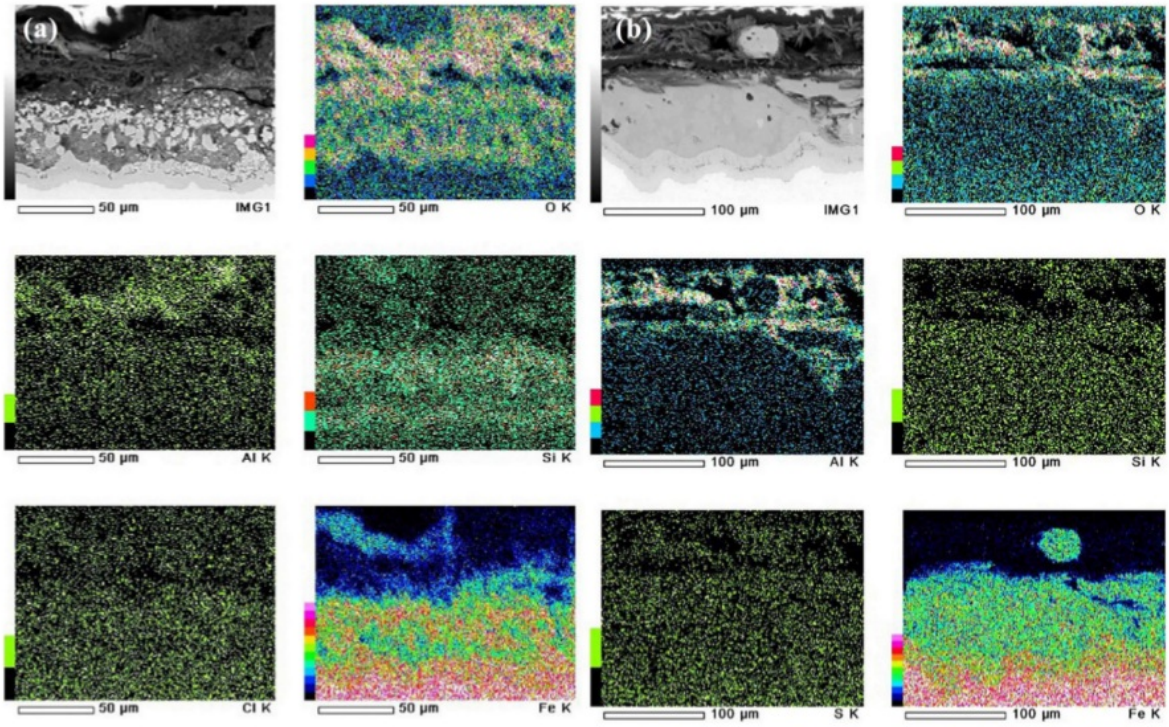

Figure 5. SEM and EDS elemental maps of AS specimens with (**a**) NaCl deposits and (**b**) Na_2SO_4 deposits, oxidized at 700°C for 49 h.

49 h, the FeAl layer replaced the Fe_2Al_5 and $FeAl_2$ layers, supplying Al atoms that formed the protective Al_2O_3 scale.

Furthermore, the presence of Na_2SO_4 deposits on the AS specimens oxidized at 700°C for 49 h had a considerable effect on the corrosion kinetics when compared with AS specimens oxidized in dry air (figure 1a). In the present study, the experimental temperature was lower than the melting point of Na_2SO_4 (884°C) [20], and the increase in weight gain was about 3.5 times that of AS oxidized in dry air (figure 1a). XRD measurements (figure 4) showed that the intermetallic phases that formed Fe_2Al_5, $FeAl_2$ and FeAl were the same in various environments. In addition, Al_2O_3 formed during the early stages of oxidation acted as a barrier to S_g, which could penetrate the aluminide layer in the reaction over short periods. Na_2SO_4 remained on the specimen surface after corrosion testing (figure 4).

As reported by Shi [17], accelerated oxidation of Fe with Na_2SO_4 deposits at 750°C may be attributed to a Na_2O/Na_2SO_4 eutectic-melt formation on the surface of the specimen. The salt decomposes when the local partial pressure of O in the environment is lower than that at equilibrium with the Na_2O/Na_2SO_4 eutectic mixture [26]. The partial pressure of O decreased because of O consumption during Al_2O_3 formation in the early stages. When the Na_2SO_4 salt that is deposited on the surface of the specimens does not melt, the following reaction tends to occur on the alumina scale [19]:

$$Na_2SO_4 \rightarrow Na_2O + SO_2 + 1/2O_2 \quad (2)$$

Subsequently, the formed $Na_2O_{(s)}$ dissolved in Na_2SO_4, reaching equilibrium with the Na_2O/Na_2SO_4 eutectic mixture [17]. The lower temperature of the eutectic mixture (550°C) [17] is strongly believed to support the formation of aluminium sulphide (Al_2S_3) in the aluminide layer by allowing the release of SO_{3g} into the atmosphere. Because Na_2SO_4 was still found on the aluminide layer surface after it was oxidized for 9 h (figure 4), the decomposition is believed to supply S that forms Al_2S_3 on the $Fe_2Al_5/FeAl_2$ layer.

Examination of the SEM cross-sectional micrographs and EDS elemental maps of O, Fe, Al, Cl and S clearly shows the difference between the effects of NaCl [15] and Na_2SO_4 deposits on AS with respect to acceleration of oxidation and corrosion (figure 5a and b). The micrograph of the corroded sample clearly shows that the aluminide $Fe_2Al_5/FeAl_2$ layer formed on the FeAl layer (figure 5b). Elemental mapping of this scale (figure 5b) suggests that the corrosion products consisted mainly of Al_2O_3 and some Fe_2O_3 scales. In the early stage of corrosion, an Al_2O_3 scale was quickly formed by unmelted Na_2SO_4 on the surface of the specimens.

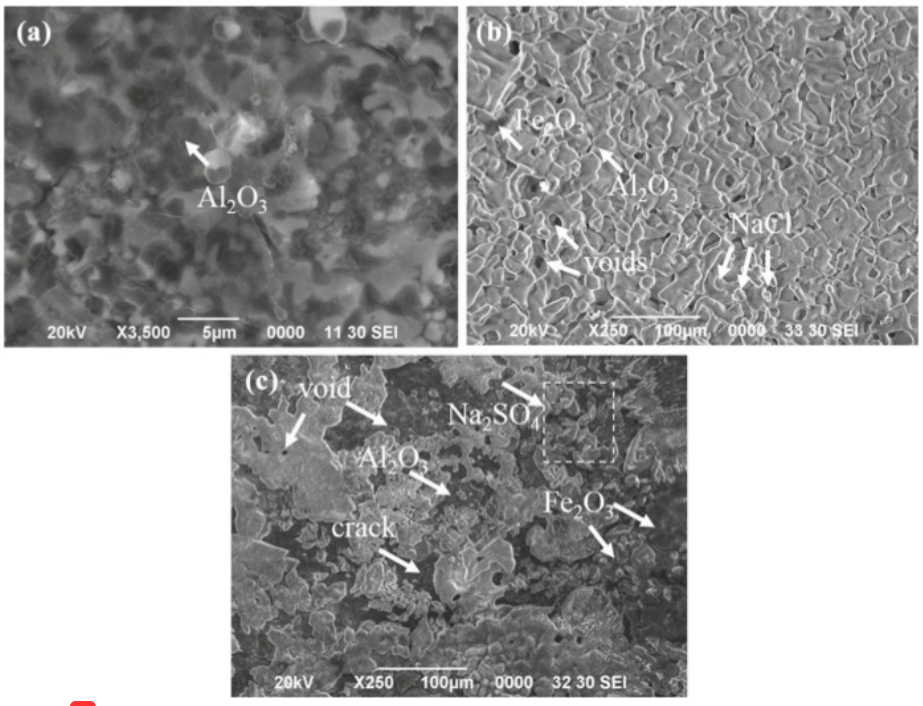

Figure 6. SEM images of the surface morphologies of AS oxidized at 700°C for 49 h (**a**) in dry air, (**b**) in an NaCl environment and (**c**) in an Na_2SO_4 environment.

SEM observation of the AS surface after oxidation in dry air at 700°C for 49 h (figure 6a) indicates that the Al_2O_3 scale on the aluminide coating is compact. In contrast, Fe_2O_3 and Al_2O_3 grew together on AS with NaCl deposits (figure 6b). Furthermore, EDS analysis of the oxide scale (figure 6c) indicated that a sulphur concentration of 10.02 wt% was sufficient to increase the high ratio of the partial pressure of S_g to the partial pressure of O_{2g} [27]. SO_3 thus released into the atmosphere diffuse and dissolve in the Al_2O_3 scale, forming $Al_2(SO_4)_3$ as confirmed by XRD (figure 4). The sulphate particles in this scale combine with the oxide matrix in the reaction over long periods. According to the Gibbs free energy ($\Delta G_{700} = -807$ kJ) given in table 1, the chemical reaction is spontaneous when sulphur ions dissolved in the aluminium oxide matrix $Al_2(SO_4)_3$ diffuse into Al_2O_3 *via* Al^{3+} vacancy defects, eventually coming into contact with Al ions diffusing from the aluminide layer. When the activities of both ions were high enough [5], Al_2S_3 forms as shown in the XRD results in figure 4. This result supports the hypothesis that Na_2SO_4 decomposition supplies S for the direct formation of trace amounts of Al_2S_3 in the oxide scale at low temperatures (such as during Na_2SO_4 melting).

EDS examination of the surface of the corroded sample (figure 6c) showed the composition in wt% in which Fe (28.17 wt%) was higher than that of Al (13.65 wt%). The composition of Al decreased because Al atoms diffused outwards to react first with oxygen, forming the Al_2O_3 scale and then diffused inwards into the steel substrate. Consequently, Al activity was decreased to a lower concentration, and the rest of the Fe reacted with the rest of the S_g remaining in the atmosphere. This result explains why SO_{3g} and O_{2g} in the atmosphere also diffused into the aluminide layer to form $FeSO_4$ in which the Fe atom activity was high. The low-formation energy of $FeSO_4$ ($\Delta G_{700} = -7.2$ kJ) facilitated $FeSO_4$ dissociation to Fe_2O_3 and subsequent release of SO_2 into the atmosphere. The reaction of sulphur gas (as SO_2) with O_{2g} in the atmosphere also produced SO_3 gas. These reactions continued cyclically, forming an Fe-rich oxide (figure 6c) and Al_2S_3 as confirmed by XRD measurements (figure 4). Consequently, Al_2O_3 failed to protect the aluminide layer and the steel substrate at 700°C during corrosion over long periods.

4. Conclusions

The presence of NaCl and Na_2SO_4 deposits on the surface of AISI 1020 steel can accelerate oxidation and corrosion. However, the aluminizing coating on the steel could cause a one to three orders of magnitude reduction in k_p for oxidation at 700°C for 49 h in an environment containing Cl_2 and S_g, relative to that of steel without the coating. During the early stages of hot corrosion, a thin and dense Al_2O_3 scale was created. During the subsequent corrosion, this Al_2O_3 layer

facilitated the formation of a porous Fe_2O_3 scale on itself, which allowed Cl and S penetration into the aluminide layer and enhanced the corrosion kinetics. Vaporization of Al_2Cl_3 and Fe_2Cl_3 is believed to strongly affect the corrosion kinetics of AS with NaCl deposits, contributing to the decrease in weight gain after oxidation for 9 h. In contrast, from Na_2SO_4 decomposition degraded the protective Al_2Cl_3 scale, allowing to easily penetrate the oxide scale and form Al_2S_3. The consequent and appreciable increase in the penetration depth of S appears to have resulted in the precipitation of sulphide particles and growth of Fe_2O_3.

Acknowledgements

The authors thank the Ministry of Research, Technology, and Higher Education of the Republic of Indonesia for financial support *via* the Incentive Research System of National Innovation and the National Strategy Research grant under contract number 529/UN26/8/LPPM/2016–2017.

References

[1] Subhash K, Jayaganthan R and Prakash S 2010 *Bull. Mater. Sci.* **33** 299
[2] Safadoost A, Davoodi M and Mansoori S A A 2014 *J. Nat. Gas Sci. Eng*. **19** 105
[3] Mishra N K and Mishra S B 2015 *Bull. Mater. Sci.* **38** 1679
[4] Lindberg D, Niemi J, Engblom M, Yrjas P, Lauren T and Hupa M 2016 *Fuel Process. Technol.* **141** 285
[5] Badaruddin M, Risano A Y E, Wardono H and Asmi D 2017 *AIP Conf. Proc*. **1788** 030066
[6] Sen M, Balasubramaniam R and Kumar A V R 2000 *Bull. Mater. Sci.* **23** 399
[7] Liu H H, Cheng W J and Wang C J 2011 *Appl. Surf. Sci.* **257** 10645
[8] Badaruddin M, Wang C J, Wardono H, Tarkono and Asmi D 2016 *AIP Conf. Proc*. **1711** 040002
[9] Wang C J and Li C C 2004 *Surf. Coat. Technol*. **177–178** 37
[10] Wang C J, Lee J W and Twu T H 2003 *Surf. Coat. Technol*. **163–164** 37
[11] Bose S 2018 High-temperature corrosion in *High temperature coating*, chapter 5, 2nd edn (Butterworth-Heinemann: Elsevier) 74. https://doi.org/10.1016/C2015-0-01316-8
[12] Yajiang L, Juan W, Yonglan Z and Holly X 2002 *Bull. Mater. Sci*. **25** 635
[13] Bouche K, Barbier F and Coulet A 1998 *Mater. Sci. Eng. A* **249** 167
[14] Pieraggi B 1987 *Oxid. Met.* **27** 177
[15] Badaruddin M and Sugiyanto 2013 *Adv. Mater. Res*. **789** 463
[16] Koech P K and Wang C J 2018 *Oxid. Met*. **90** 713
[17] Shi L 1993 *Oxid. Met*. **40** 197
[18] Ciszak C, Popa I, Brossard J M, Monceau D and Chevalier S 2016 *Corros. Sci*. **110** 91
[19] Yan Y F, Xu X Q, Zhou D Q, Wang H, Wu Y, Liu X J *et al* 2013 *Corros. Sci*. **77** 202
[20] Speight J G 2002 *Lange's handbook of chemistry* 16th edn (New York: McGraw-Hill)
[21] Godlewska E, Mitoraj M and Leszczynska K 2014 *Corros. Sci*. **78** 63
[22] Knacke O, Kubaschewski O and Hesselmann K 1977 *Thermochemical properties of inorganic substance* (Berlin: Springer) 91. https://doi.org/10.1007/978-3-662-02293-1
[23] Neumann G 1990 in *Diffusion in solid metals and alloys, numerical data and functional relationships in science and technology* H Mehrer (ed) (Springer-Verlag, Berlin) vol. 26, p 152
[24] Le Claire A D 1990 in *Diffusion in solid metals and alloys, numerical data and functional relationship in science and technology* H Mehrer (ed) (Springer-Verlag, Berlin) vol. 26, p 129
[25] Tsaur C C, Rock J C, Wang C J and Su Y H 2005 *Mater. Chem. Phys*. **89** 445
[26] Buscaglia V, Nanni P and Bottino C 1990 *Corros. Sci*. **30** 327
[27] Lee W H and Lin R Y 1999 *Mater. Chem. Phys*. **58** 231

High-temperature corrosion of aluminized-AISI 1020 steel with NaCl and Na2SO4 deposits

ORIGINALITY REPORT

80%

SIMILARITY INDEX

PRIMARY SOURCES

1	link.springer.com Internet	3350 words — 77%
2	Y.F. Yan, X.Q. Xu, D.Q. Zhou, H. Wang, Y. Wu, X.J. Liu, Z.P. Lu. "Hot corrosion behaviour and its mechanism of a new alumina-forming austenitic stainless steel in molten sodium sulphate", Corrosion Science, 2013 Crossref	37 words — 1%
3	Onkar Mangla, Savita Roy, S Annapoorni, K Asokan. "A study on defect annealing in GaAs nanostructures by ion beam irradiation", Bulletin of Materials Science, 2020 Crossref	36 words — 1%
4	repository.lppm.unila.ac.id Internet	13 words — < 1%
5	Susan Immanuel, R Sivasubramanian. "Fabrication of two-dimensional chemically reduced graphene oxide nanosheets for the electrochemical determination of epinephrine", Bulletin of Materials Science, 2020 Crossref	13 words — < 1%
6	www.kemija.org Internet	10 words — < 1%
7	Singh, H.. "Characterization of oxide scales to evaluate high temperature oxidation behavior of Ni-20Cr coated superalloys", Materials Science & Engineering A, 20070825 Crossref	9 words — < 1%

8	homer.ugdsb.on.ca Internet	8 words — < 1%
9	Rodrigo Cardoso Costa, Michel Volpato Dacoreggio, Norton Zanette Kejelin, Franco Wronski Comeli. "Avaliação da resistência a corrosão de revestimentos metálicos depositados por aspersão térmica a arco: uma aplicação em trocadores de calor", Soldagem & Inspeção, 2014 Crossref	8 words — < 1%
10	M. Reza Bateni, Stephanie Shaw, Ping Wei, Anthony Petric. "Deposition of Fe–Al Intermetallic Coatings on Solid Oxide Fuel Cell (SOFC) Interconnects by Pack Cementation", Materials and Manufacturing Processes, 2009 Crossref	8 words — < 1%
11	Mohammad Badaruddin, Chaur Jeng Wang, Yudhistyra Saputra, Abu Khalid Rivai. "High Temperature Corrosion of Aluminized AISI 4130 Steel with the Different Composition of NaCl/Na2SO4 Deposits", Makara Journal of Technology, 2015 Crossref	6 words — < 1%

EXCLUDE QUOTES	ON	EXCLUDE MATCHES	OFF
EXCLUDE BIBLIOGRAPHY	ON		